IET Electric Power Applications

Research Article

IET Journals
The Institution of Engineering and Technology

Performance prediction of surface-mounted permanent magnet synchronous motor based on ring specimen test result

ISSN 1751-8660
Received on 28th June 2018
Revised 21st December 2018
Accepted on 11th March 2019
doi: 10.1049/iet-epa.2018.5382
www.ietdl.org

Dong-Min Kim[1], Jun-Woo Chin[1], Jung-Pyo Hong[1], Myung-Seop Lim[1] ✉

[1]*Department of Automotive Engineering, Hanyang University, 04763, Seoul, Republic of Korea*

✉ *E-mail: limmang87@hanyang.ac.kr*

Abstract: The B–H curve and iron loss of electrical steel sheets are essential data for predicting the performance of electric motors. The Epstein frame test is widely adopted to acquire these magnetic properties. However, for rotating electric machines with relatively small geometry, the ring specimen test is preferred because of its simplicity and geometric similarity. This study deals with the experimental verification of the ring specimen test. The B–H curve and iron loss of non-oriented electrical steel sheets are measured via the Epstein frame test and the ring specimen test. Each result is applied in finite element analysis (FEA) of the fabricated electric motor. Furthermore, using these FEA results and the *d*-*q*-axis equivalent circuit, the performance of the electric motor is predicted. For experimental verification, electric motor tests are performed under no-load and load conditions.

1 Introduction

The flux of magnetic circuits in electric machines mainly passes through the core, which consists of an electrical steel sheet. Therefore, the magnetic properties of the electrical steel sheet must be known to predict the performance of electric machines. The permeability of the electrical steel sheet and losses significantly influence the performance of the electric machine. For rotating electric machines, the loss can be divided into copper loss induced by the winding, iron loss occurring at the electrical steel sheet, and mechanical loss caused by the bearing and air friction. Among these, the permeability and iron loss are related to the characteristics of the electrical steel sheet. Thus, the iron loss and B–H curve of electrical steel sheets are needed for predicting the performance of electric machines.

Many studies on the magnetic properties of electrical steel sheets have been performed. The research topics can be roughly divided into the following three categories: B–H curve measurement, iron loss measurement, and iron loss modelling. B–H curve measurement has been studied for a very long time. Recently, in Akiror *et al.* performed B–H curve measurement for large synchronous machines [1]. Clerc and Muetze studied the degradation of the B–H curve according to the manufacturing process [2]. Although the study is not up to date, Modrijan *et al.* suggested a B–H analyser with high precision that mitigated the total harmonic distortion of the induced voltage of the secondary winding [3]. Researches about rest of major topics are considering the iron loss. Stupakov *et al.* and Telini *et al.* examined an iron loss measurement technique [4, 5]. Several studies have considered the influence of the manufacturing process on the iron loss. Imamori *et al.* demonstrated the effect of the interlocking process on the iron loss, fixing iron cores [6]. The impact of the annealing process on the iron loss was analysed by Cossale *et al.* [7]. Xue *et al.* focused on the effect of the temperature on the iron loss [8]. Several researches have studied iron loss modelling. Alatawneh *et al.* presented an accurate iron loss model that can consider a pulse width modulation waveform [9]. Hamzehbahmani *et al.* suggested a precise eddy current loss component of the iron loss model [10].

The previous explanations show that there have been numerous studies on the measurement and modelling of magnetic properties. Moreover, performance prediction has been performed considering iron loss model and non-linearity of electrical steel sheet [11, 12]. However, there have been few studies on the comparison of the magnetic properties from the Epstein frame test and the ring specimen test, through the performance test of the rotating electric machine. For anticipating the electric motor performance, the magnetic properties of electrical steel sheets should be acquired via the Epstein frame test or the ring specimen test according to the international standard [13]. The data for electrical steel sheets supplied by the manufacturer is usually acquired via the Epstein frame test. However, the ring specimen test is preferred for predicting the performance of relatively small sized rotating electrical machines, for the following reasons [14].

i. It employs a closed magnetic circuit without any air gaps.
ii. There is no need for a special measurement set.
iii. The preparation of the test is simple.
iv. The proportion of machined area in the iron core is more similar to small geometry motor core.

Compared with the Epstein frame test, the ring specimen test is simple and allows the easy preparation of specimens for testing. Moreover, the ring specimen test can offer a continuous circumferential magnetic flux path without any air gap, resulting in a uniform distribution of the magnetic flux, which allows the magnetic field intensity to be calculated accurately. In addition, the proportion of cutting area versus non-machined area is more similar to small geometry motor.

This study involves the performance prediction of the surface-mounted permanent magnet synchronous motor (SPMSM) and the measurement of the magnetic properties required for prediction through the ring specimen test. Furthermore, to achieve the objective of this paper, experimental verifications are performed via no-load and load tests. In this process, a non-oriented electrical steel sheet is used for the ring specimen test. To minimise the effects of the manufacturing process, the electrical discharge machining (EDM) wire-cut is adopted for preparing the specimen. Using the ring specimen, the B–H curve and iron losses are measured. According to these magnetic properties, the electric motor performance is predicted through finite element analysis (FEA). This process is essential to predict the motor characteristics from the measured properties. To verify the prediction results, an electric motor is introduced. No-load tests are conducted for confirmation of the B–H curve and no-load iron loss. Load tests are performed for substantiation of the performance prediction, including the iron loss under the specific load condition. Finally, the error of the test results with respect to the simulation results is examined.

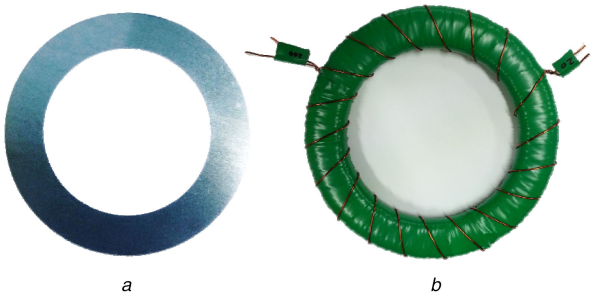

Fig. 1 *Electrical steel sheet specimen for ring specimen test*
(a) Single sheet, ***(b)*** Stacked and wound

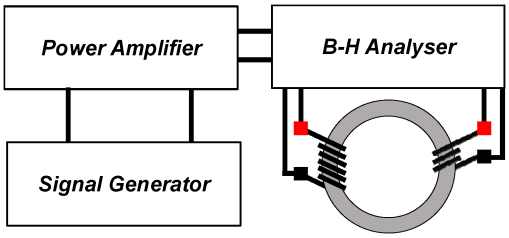

Fig. 2 *Ring specimen test set acquiring magnetic properties*

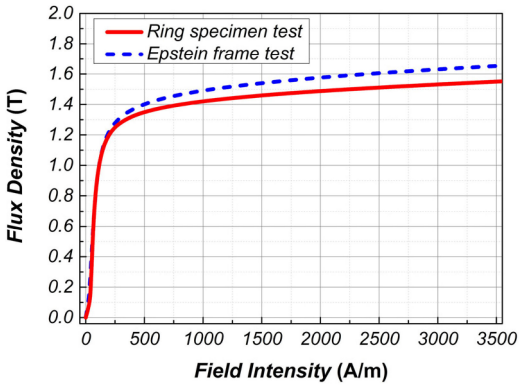

Fig. 3 *B–H curve from ring specimen test and Epstein frame test*

2 Magnetic property acquisition

To predict the characteristics of electric machines, the B–H curve and iron loss according to the magnetic flux density and operating frequency are needed. In this paper, '50PN470' is adopted for examination. This is a non-oriented electrical steel sheet with the thickness of 0.5 mm that is widely used for electric machines. In this chapter, using the ring specimen test, the B–H curve and iron loss of '50PN470' are assessed. Moreover, the magnetic properties from the Epstein frame test results supplied by the manufacturer are prepared for comparison with the ring specimen test results. At this time, the residual induction of permanent magnet is assumed as the nominal value of the catalogue, and recoil permeability is supposed constant as 1.05.

2.1 Ring specimen test

To exclude the difference of the magnetic properties according to the manufacturing process, the wire cut is adopted for preparation. Moreover, for ensuring the reliability of the test, the outer diameter of the ring specimen does not exceed 1.4 times the inner diameter [15]. Fig. 1 shows the prepared specimen, which has an outer diameter of 130 mm and an inner diameter of 100 mm. As shown in Fig. 1*b*, 20 sheets are stacked and wound. For the primary winding, 200 turns are wound with a uniform interval inside the green tape. For the secondary winding, 20 turns are wound on the green-taped surface. The primary winding of the ring specimen is connected to an alternating current (AC) voltage source and a B–H analyser. This connection can supply the appropriate magnetic field intensity by monitoring the B–H analyser. The secondary winding of the ring specimen is connected to the B–H analyser to measure the magnetic flux density using the induced voltage. An NF high-speed power amplifier was used as the AC voltage source, and an IWATSU SY8258 B–H analyser was used for measuring the B–H curves and iron losses. This B–H analyser employed the cross-power method (IEC 62044-3) and had a frequency range of 50 Hz – 1 MHz, with 0.1% precision [16]. (Fig. 2)

2.2 B–H curve

To assess the B–H characteristics of the electrical steel sheet, the initial direct current (DC) magnetisation curve was measured using (1) and (2). N_1 and N_2 represent the number of turns of the primary and secondary windings, respectively; and V_1, I_1 and V_2, I_2 represent the voltage and current of the primary and secondary windings, respectively. A is the cross-sectional area, and l is the effective length of the magnetic flux path of the ring specimen [17]. The test range of the magnetic flux density is 0.1–1.6 T, and accordingly the intensity range of the applied field is 35.61–4,956 A/m. To measure an accurate B–H curve, the frequency of the applied magnetomotive force should be measured at a frequency close to zero. In this study, the measurement was performed at 50 Hz owing to the limitations of the measuring equipment. Therefore, we proceeded to predict the characteristics of the SPMSM, where the main magnetic flux was produced by permanent magnets. Its electrical air-gap length was relatively large. In Fig. 3, the B–H curve obtained from this test is depicted as a solid red line. For comparison, the Epstein frame test result is depicted as a blue dashed line.

$$H(t) = \frac{N_1 \cdot I_1(t)}{l} \tag{1}$$

$$B(t) = \frac{1}{N_2 A} \int V_2(t)\,\mathrm{d}t \tag{2}$$

2.3 Iron loss

The iron loss was measured using the same method that was used for the B–H curve assessment, except that the measuring frequency was changed. Using (3), the iron loss P_c was calculated according to the frequency f. The tests were conducted in the magnetic flux density range of 0.1–1.8 T and the frequency range of 50 to 1,000 Hz.

$$P_c = \frac{1}{A \cdot l} \times \frac{N_1}{N_2} \times f \times \int_0^T I_1(t) \times V_2(t)\,\mathrm{d}t \tag{3}$$

For predicting the electric motor performance, the iron loss surface interpolated and extrapolated from each test using Steinmetz's equation and the least squares method is shown in Fig. 4 [18]. The error between the results of the ring specimen test and the Epstein frame test can be caused by the machining process and the difference in the direction of the magnetic flux path. To describe the magnetic flux direction in additional detail, in the Epstein frame test, the direction of the magnetic flux path is the same as the rolling direction of the electrical steel sheet except for the corner intersections. However, in the ring specimen test, the angle between the magnetic flux path and the rolling direction of the electrical steel sheet varies according to the position [14]. According to Steinmetz's equation, the iron loss can be modelled using (4), where B represents the magnetic flux density, and f represents the frequency. The coefficients k_a, k_e, and k_h represent the anomalous loss, eddy current loss, and hysteresis loss components, respectively.

$$W_{\text{iron}} = k_a \times f^{1.5} \times B^{1.5} + k_e \times f^2 \times B^2 + k_h \times f \times B^2 \tag{4}$$

The frequency range for extrapolation is determined considering the maximum operating speed of the target motor. As shown in Table 1, the maximum speed of the target motor is 3,500 RPM with 10 poles. From this condition, the maximum electrical

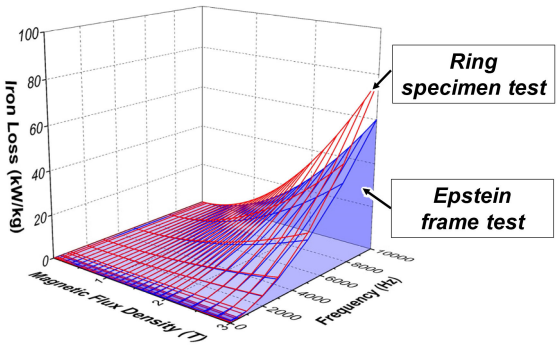

Fig. 4 *Interpolated and extrapolated iron loss surface from Epstein frame test result and ring specimen test result*

Table 1 Specification of target motor

Items	Value	Unit
type	SPMSM	—
pole number	10	—
slot number	12	—
stator outer diameter	107	mm
stack length	44	mm
core material	50PN470	(Density: 7700 kg/m^3)
magnet material	NdFeB	(Density: 7500 kg/m^3)
rated power	380	W (@1800RPM)
maximum speed	3500	RPM
maximum torque	2	Nm

Table 2 Curve fitting result of iron loss for Steinmetz's equation

	Frequency, Hz								
Coefficient	30	60	100	150	200	400	600	800	1000
k_a (10×10^{-3})	0.154	0.147	0.087	0.065	0.069	0.068	0.061	0.059	0.054
k_e (10×10^{-3})	0.832	0.508	0.390	0.327	0.286	0.235	0.211	0.186	0.156
k_h (10×10^{-3})	1.386	1.118	0.823	0.705	0.673	0.510	0.421	0.316	0.211
r-square	0.994	0.997	0.998	0.998	0.997	0.993	0.989	0.987	0.994

Table 3 Coefficients fitting result according to frequency

	k_a	k_e	k_h
M	0.000052	0.000063	0.000070
N	0.002470	0.005615	0.007575
P	0.9	0.6	0.5
R-square	0.866	0.986	0.973

fundamental frequency is calculated as 291.67 Hz. To consider the 30th order harmonic component, the frequency range for extrapolation should be above 8,750 Hz. Therefore, the frequency range is set as 10,000 Hz.

First, using the least squares method, the measured iron loss is subjected to curve fitting with B as a domain via (4). At this time, the coefficients k_a, k_e, k_h are determined for each frequency f, maximising the R-square, i.e. the coefficient of determination. For the next step, using the coefficients k_a, k_e, k_h determined for each frequency, curve fitting is performed by using the frequency f as a domain. In this case, curve fitting is conducted using the least squares method in the form of $m + nx^{-p}$. The value of the coefficient p is determined to maximise the R-square value in the range of 0.5–1.0 for each of the coefficients k_a, k_e, k_h, as described in (5). The curve fitting results are shown in Tables 2 and 3. Consequently, the iron loss can be expressed by (6).

$$\begin{cases} k_a = m_a + \dfrac{n_a}{f^{p_a}} \\ k_e = m_e + \dfrac{n_e}{f^{p_e}} \\ k_h = m_h + \dfrac{n_h}{f^{p_h}} \end{cases} \tag{5}$$

$$\begin{aligned} W_{iron} = &\left(m_a + \frac{n_a}{f^{p_a}}\right) \times f^{1.5} \times B^{1.5} \\ &+ \left(m_e + \frac{n_e}{f^{p_e}}\right) \times f^2 \times B^2 + \left(m_h + \frac{n_h}{f^{p_h}}\right) \times f \times B^2 \end{aligned} \tag{6}$$

3 Electric motor characteristics

An SPMSM type target motor is employed for verification of the ring specimen test results. Detailed specifications of the target SPMSM are presented in Table 1. The target motor is fabricated using wire-cut as same as the ring specimen preparation. The welding is adopted to fix the stator core lamination. However, the welding position does not disturb the flux. Two-dimensional (2D) FEA is used, and the 2D FEA model of the target motor is described in Fig. 5. Predictions are made for the no-load and load conditions. The predicted results are compared with the experimental results in Chapter 4.

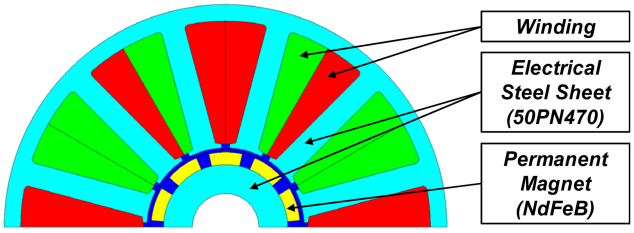

Fig. 5 *2D FEA anti-periodic model of target motor*

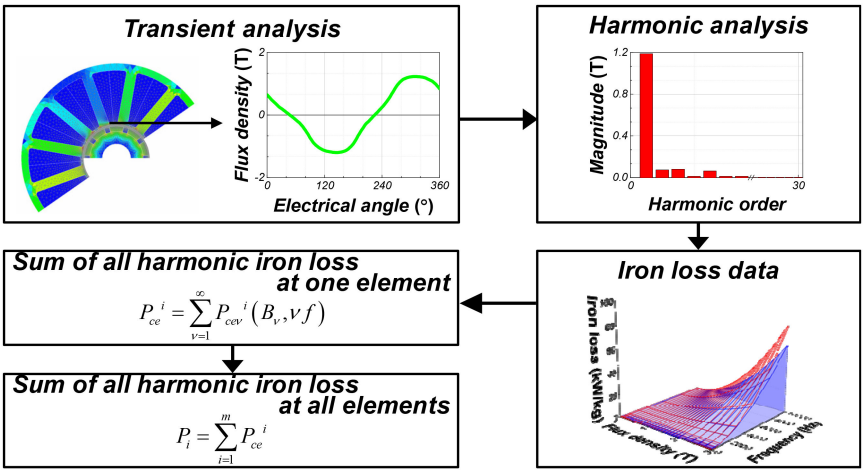

Fig. 6 *Iron loss calculation process*

3.1 No-load condition characteristics

To validate the measured B–H curve, the no-load back electromotive force (back EMF) is calculated using 2D FEA with the B–H curves previously acquired from the Epstein frame test and the ring specimen test. The no-load iron loss calculation is also performed, for comparison with the iron loss measurement test results in Section 4.1 of Chapter 4. Fig. 6 shows the calculation process for the iron loss. First, to assess the no-load iron loss, the magnetic flux density at the position of each element is calculated under the no-load condition of 2D FEA. Next, the calculated magnetic flux density distribution is subjected to harmonic analysis through a Fourier transform. Then, using the interpolated and extrapolated iron loss surface shown in Fig. 4, the harmonic iron losses for each element are calculated and summed. The total iron loss for all elements is the no-load iron loss. In the next section, this iron loss calculation process proceeds in the same way, with the conditions changing from no-load conditions to load conditions [19, 20]. The adopted iron loss calculation process assumed that the iron loss of the harmonic component is equal to the iron loss caused by the fundamental wave having that harmonic magnitude. In order to calculate the iron loss exactly, it is necessary to measure the iron loss using the current waveform including harmonics [21, 22]. Otherwise, the hysteresis loop model should be considered. However, it is difficult to measure the iron loss for all situations including harmonics, and it is difficult to use the hysteresis model in terms of computing cost and model verification. As of these problems, studies using the combined method are also underway [23], but the method used in this paper also has no problem in predicting iron loss [24]. The introduced iron loss calculation process is more suitable for the prediction of performance according to the wide range of operating points than other processes.

3.2 Load condition characteristics

The performance of the electric motors is predicted by the *d*-*q*-axis equivalent circuit of the permanent magnet synchronous motors (PMSMs), considering the iron loss. The *d*-*q*-axis equivalent circuit is used to predict the electric motor characteristics such as input current for the range of speed and torque. This allows easy derivation of the solution because it converts three-phase AC voltage equation to simple DC voltage equation. The rotating reference frame is applied in this transformation. This equivalent circuit can be applied to any synchronous motor such as interior permanent magnet synchronous motor (IPMSM) or SPMSM [20, 25]. Using 2D FEA, the *d*-axis and *q*-axis inductances are calculated for the range of the input current. In the inductance calculation process, for the same range, the linkage flux of the armature winding is calculated. The reason of *d*-*q*-axis inductance calculation for the SPMSM is to improve the precision. Generally, the SPMSM is known as a non-salient motor. However, because of the effect of magnetic saturation and little difference of permeability between the PM and air, there exists the little difference between the *d* and *q*-axis inductance. Furthermore, for the same range, the iron loss is calculated using the process shown in Fig. 6. After the parameter calculation process, the *d*-*q*-axis equivalent circuit of the PMSM is solved for the speed and torque range, considering the DC-link voltage and current limitation. This process is conducted two times for the Epstein frame test result and the ring specimen test result. As a result, two electric motor characteristic curves are created for each test [25]. When solving the *d*-*q*-axis equivalent circuit, the voltage equation can be given by (7) and (8). R_a is the phase resistance of the stator winding, and L_d and L_q are the *d*- and *q*-axis inductances, respectively. R_{iron} is the equivalent iron loss resistance for the acting iron loss component in the *d*-*q* equivalent circuit. $\mathrm{i_{od}}$, $\mathrm{i_{oq}}$, and v_{od}, v_{oq} represent the magnetising *d*-axis and *q*-axis currents and the corresponding voltages. *p* is the differential operator.

$$\begin{bmatrix} v_{\mathrm{d}} \\ v_{q} \end{bmatrix} = R_a \begin{bmatrix} \mathrm{i_{od}} \\ \mathrm{i_{oq}} \end{bmatrix} + \left(1 + \frac{R_a}{R_{\text{iron}}}\right) \begin{bmatrix} v_{\text{od}} \\ v_{\text{oq}} \end{bmatrix} + p \begin{bmatrix} L_{\mathrm{d}} & 0 \\ 0 & L_q \end{bmatrix} \begin{bmatrix} \mathrm{i_{od}} \\ \mathrm{i_{oq}} \end{bmatrix} \tag{7}$$

$$\begin{bmatrix} v_{\text{od}} \\ v_{\text{oq}} \end{bmatrix} = \begin{bmatrix} 0 & \omega \mathrm{L_q} \\ \omega \mathrm{L_d} & 0 \end{bmatrix} \begin{bmatrix} \mathrm{i_{od}} \\ \mathrm{i_{oq}} \end{bmatrix} + \begin{bmatrix} 0 \\ \omega \Psi_a \end{bmatrix} \tag{8}$$

By examining the relationship between iron loss and the equivalent iron loss resistor, (9) can be generated, as shown below. Here, V_o shows the induced voltage of the armature winding.

$$W_{\mathrm{i}} = \frac{V_o^2}{R_{\text{iron}}} = \frac{v_{\text{od}}^2 + v_{\text{oq}}^2}{R_{\text{iron}}} = \frac{\omega^2 \left\{ (L_{\mathrm{d}} \mathrm{i_{od}} + \Psi_a)^2 + (L_q \mathrm{i_{oq}})^2 \right\}}{R_{\text{iron}}} \tag{9}$$

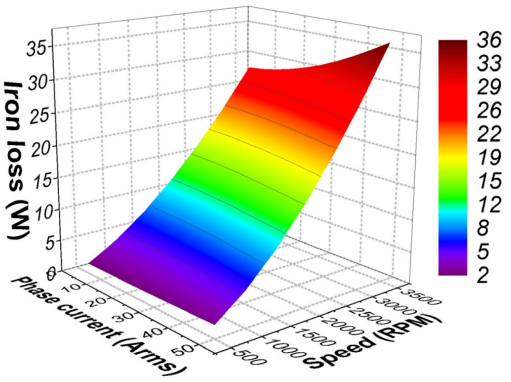

Fig. 7 *Calculated iron loss according to input current and operating speed*

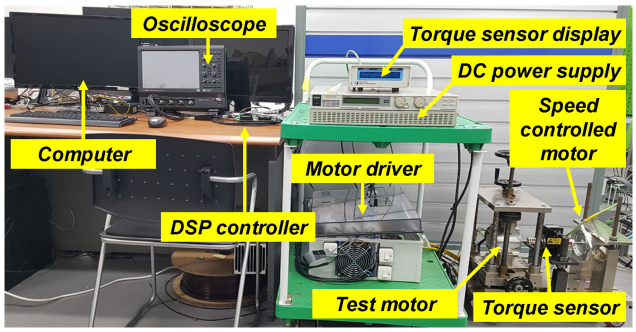

Fig. 8 *No-load test set*

From these relationships, the torque equation can be derived as (10), where P_n is the number of the pole pairs, and Ψ_a is the linkage flux of the armature. This equation can be separated into two terms: the magnetic torque, $P_n\Psi_a i_{oq}$, and the reluctance torque, $(L_d–L_q)i_{od}i_{oq}$.

$$T = P_n\{\Psi_a i_{oq} + (L_d - L_q)i_{od}i_{oq}\} \quad (10)$$

Moreover, as a result of the addition of the iron loss equivalent resistor, i_{cd} and i_{cq} occur, flowing the iron loss equivalent resistor of the *d*-axis and *q*-axis equivalent circuit. In this way, the *d*-axis current i_d and *q*-axis current i_q can be formulated according to (12) and (13), respectively. In conclusion, the phase current I_a can be calculated using (14). This process conducted for each operating point including *d*-*q*-axis inductances and W_i and R_{iron}. Fig. 7, shows the calculated iron loss according to the input current and operating speed.

$$i_d = i_{od} + i_{cd} \quad (11)$$

$$i_q = i_{oq} + i_{cq} \quad (12)$$

$$I_a = \sqrt{i_d^2 + i_q^2} \quad (13)$$

4 Experimental verification

4.1 No-load test

The no-load test set is formed as shown in Fig. 8. In the beginning, a jig is prepared that can fix the test motor and adjust the three-axis position. Then, the torque sensor '*TM303*' from Magtrol is equipped. The nominal rated torque is 0.5 Nm, with 0.1% accuracy of the rated torque. The speed detection resolution is 1 RPM. Finally, a speed-controlled external drive motor is joined to the torque sensor shaft at the opposite side of the test motor. This speed-controlled motor is connected to the motor driver, and the motor driver is connected to the computer by a DSP controller. The desired test speeds are entered through this controller, and its status is monitored by an oscilloscope.

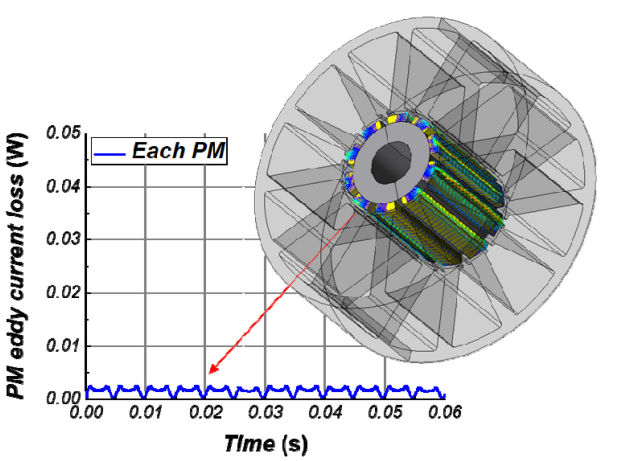

Fig. 9 *3D FEA result of eddy current loss of each permanent magnet at no-load condition*

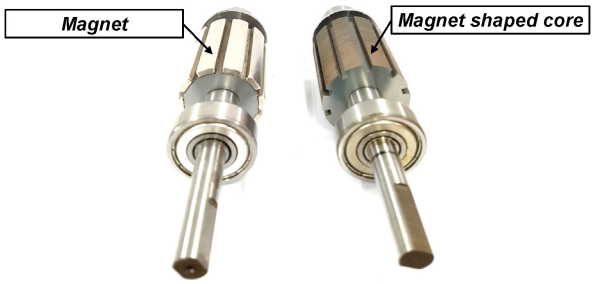

Fig. 10 *Original rotor (left) with surface mounted magnet and rotor for iron loss separation (right) with magnet shaped core*

First, the no-load back EMF at 1,000 RPM is measured. Before the measurement, continuous driving is performed at 1,000 RPM for 5 min. This procedure can minimise the transient effect of the bearing and thermal condition. At this time, the temperature variation of permanent magnet is not considered, because of the eddy current loss of the permanent magnet at no-load condition is very low. In Fig. 9, 3D FEA result of permanent magnet eddy current loss is depicted. In Table 4 in Chapter 5, the measured no-load back EMF is compared with the predicted result from Section 3.1 of Chapter 3.

Then, the iron loss is measured. This test is conducted using the rotors described in Fig. 10. The left one is the initially assembled rotor with the permanent magnet, mounted on the surface of the rotor. The right one is the rotor with the magnet shaped core. In this section, the former is called the 'original rotor,' and the latter is called the 'non-magnetised rotor.' The procedure of the iron loss measurement is described as follows:

(1) Install the test motor with the original rotor, aligned to the axis of the torque sensor shaft.
(2) Drive the test motor for 5 min by using the speed-controlled motor at 1,000 RPM in a no-load condition.
(3) Drive the test motor for 100 s by using the speed-controlled motor at 500 RPM in a no-load condition.
(4) Simultaneously, log the data from the torque sensor and calculate the average value of the measured data.
(5) Allow the motor to rest for 10 min.
(6) Repeat steps (2)–(5) until the test speed of the third process is changed to 3,500 RPM in increments of 500 RPM.
(7) Change the rotor to the non-magnetised rotor and repeat the preceding process.

The data logged in step (4) can be transformed into a no-load loss at a specific rotational speed. Multiplying the measured torque by the test speed results in a no-load loss. The result of the test with the original rotor is the combination of the mechanical loss and no-load iron loss. The result of switching to the non-magnetised rotor

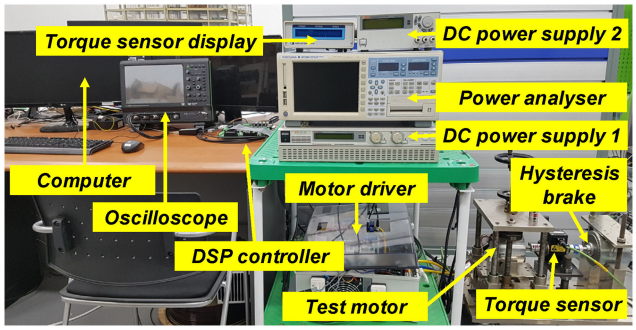

Fig. 11 *Load test set*

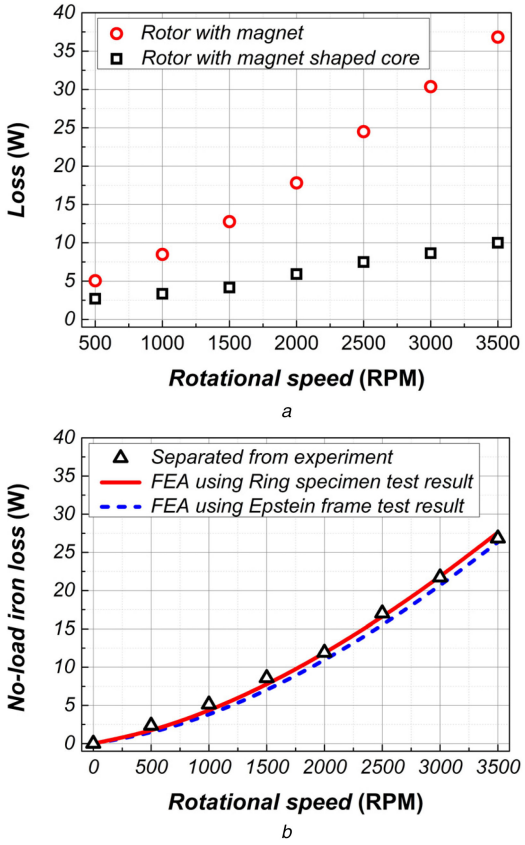

Fig. 12 *Loss separation test results*
(a) Comparison of no-load loss between rotor wit magnet and rotor with magnet shaped core, ***(b)*** Iron loss separation result with FEA results using each test results

is the mechanical loss. Subtracting the test results for the non-magnetised rotor from the test results for the original rotor results in a no-load iron loss. These results are verified in Fig. 12 of Chapter 5.

4.2 Load test

To verify the load-condition prediction in Section 3.2 of Chapter 3, the ring specimen test results are used, and a load test is performed. The load-test set is described in Fig. 11. Instead of the speed-controlled motor in the no-load test set, the hysteresis brake is equipped with an additional DC power supply. Furthermore, to measure the input current of the test motor and to monitor the driving status, the power analyser '*WT3000*' from Yokogawa is added and wired in a three-phase four-wired configuration. After the test bench setup, the load test is conducted to obtain the maximum performance curve. The test result is examined in Table 5 and Fig. 13 of Chapter 5.

5 Result

From the no-load test, the no-load back EMF at 1,000 RPM and iron loss are determined, as shown in Figs. 12 and 13. Fig. 12

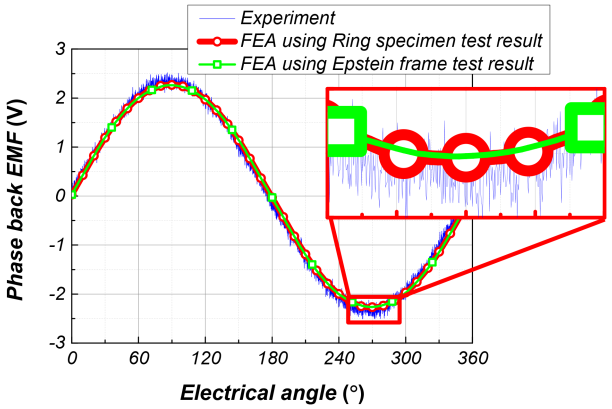

Fig. 13 *No-load back EMF comparison between experimentally measured result and estimated results*

Table 4 Measured no-load back EMF and estimated result

Items	Experiment	Ring	Epstein
back EMF (V_{RMS})	1.644	1.618	1.620
error (%)	—	1.582	1.460

shows that the no-load iron loss is well estimated by 2D FEA using the ring specimen test result and Epstein frame test result. Fig. 13 shows that the no-load back EMF estimation is accurate enough to make it difficult to distinguish between the experimental and estimated no-load back EMFs. In Table 4, the back EMF measurement result is examined. The measured root mean square (RMS) value of the fundamental component of the no-load back EMF at 1,000 RPM is 1.644 V. The values predicted using the ring specimen test result and the Epstein frame test result are 1.618 and 1.620 V, respectively. The load test also exhibits respectable results. Table 5 shows the load test point and measured values. In Fig. 14, the torque-speed-current curve is compared between the experiment and the estimated results. The black square and the red circle represent the measured operating point and the corresponding measured current, respectively. From this measured current, extrapolation is performed, as indicated by the red dashed line. For comparison, a solid black line representing the estimated operating points, as well as a thick solid blue line and a blue dotted line representing the currents estimated using the ring specimen test result and Epstein frame test result, respectively, are depicted. These are RMS values of the input phase current in amperes. These lines show that the predicted input current for the operating points is within a sufficiently tolerable error range.

6 Conclusion

This paper presented experimental verification of ring specimen test results applied to a target SPMSM. The magnetic properties were measured through the ring specimen test, and the performances of the target motor were predicted using these data for the no-load condition and several load conditions. For validation, the no-load back EMF and the no-load loss were measured. Moreover, the load test was conducted along the maximum output performance curve. According to the results of these validations, the ring specimen test results are comparable to the results of the Epstein frame test. FEA performed using the ring specimen test results indicated that the error with respect to the measured value was <1.6% for the no-load back EMF, and the iron loss prediction result under the no-load condition was 7.8% closer to the loss separation test result than the result obtained using the Epstein frame test. This aspect is also observed in the load test. The difference between the RMS value of the input current measured at the experimental points and the characteristic analysis results obtained using the ring specimen test ranged from 2% to 3.6%, and the average value of the difference was 2.8%. The difference from the characteristics analysis results obtained using the Epstein frame test ranged from 2.9% to 4.8%, with an average value of 3.9%. Considering the experimental error, both the Epstein frame test

Table 5 Load test result and comparison

Experiment point			Input current (A_{RMS})	
Speed, rpm	Torque, Nm	Experiment	Ring (error)	Epstein (error)
500.00	2.00	46.93	45.53 (2.98)	44.98 (4.16)
1000.00	2.00	47.02	45.32 (3.62)	44.78 (4.76)
1500.00	2.00	46.71	45.38 (2.85)	44.85 (3.98)
2000.00	1.80	42.26	41.12 (2.70)	40.67 (3.76)
2500.00	1.44	33.99	33.31 (2.00)	32.99 (2.94)

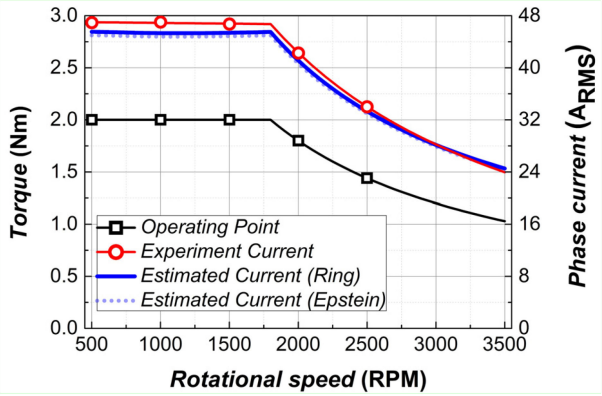

Fig. 14 *Measured TNI curve from load test and correspond estimated result from 2D FEA using Ring specimen test and Epstein frame test result*

result and the ring specimen test result were meaningful. Therefore, it is sufficient to use the ring specimen test to predict the motor performances.

7 Acknowledgments

This research was financially supported by the Ministry of Trade, Industry, and Energy (MOTIE), Korea, under the 'Commercializing fuel cell electric vehicle component industry and R&D Support Program'(reference number R0006468) supervised by the Korea Institute for Advancement of Technology (KIAT).

8 References

[1] Akiror, J.C., Pillay, P., Merkhouf, A.: 'Challenges in modeling of large synchronous machines', *IEEE Trans. Ind. Appl.*, 2018, **54**, (2), pp. 1652–1662

[2] Clerc, A.J, Muetze, A.: 'Measurement of stator core magnetic degradation during the manufacturing process', *IEEE Trans. Ind. Appl.*, 2012, **48**, (4), pp. 1344–1352

[3] Modrijan, G., Petkovsek, M., Zajec, P., *et al.*: 'Precision B-H analyzer with low THD secondary induced voltage', *IEEE Trans. Ind. Electron.*, 2008, **55**, (1), pp. 364–370

[4] Stupakov, O., Wood, R., Melikhov, Y., *et al.*: 'Measurement of electrical steels with direct field determination', *IEEE Trans. Magn.*, 2010, **46**, (2), pp. 298–301

[5] Tellini, B., Giannetti, R., Lizon-Martinez, S.: 'Characterization of the accommodation effect in soft hysteretic materials via sensorless measurement technique', *IEEE Trans. Instrum. Meas.*, 2009, **58**, (8), pp. 2807–2814

[6] Imamori, S., Steentjes, S., Hameyer, K.: 'Influence of interlocking on magnetic properties of electrical steel laminations', *IEEE Trans. Magn.*, 2017, **53**, (11), pp. 1–4

[7] Cossale, M., Krings, A., Soulard, J., *et al.*: 'Practical investigations on cobalt-iron laminations for electrical machines', *IEEE Trans. Ind. Appl.*, 2015, **51**, (4), pp. 2933–2939

[8] Xue, S., Chu, W.Q., Zhu, Z.Q., *et al.*: 'Iron loss calculation considering temperature influence in non-oriented steel laminations', *IET Sci. Meas. Technol.*, 2016, **10**, (8), pp. 846–854

[9] Alatawneh, N., Rahman, T., Hussain, S., *et al.*: 'Accuracy of time domain extension formulae of core losses in non-oriented electrical steel laminations under non-sinusoidal excitation', *IET Electr. Power Appl.*, 2017, **11**, (6), pp. 1131–1139

[10] Hamzehbahmani, H., Anderson, P., Preece, S.: 'Application of an advanced eddy-current loss modelling to magnetic properties of electrical steel laminations in a wide range of measurements', *IET Sci. Meas. Technol.*, 2015, **9**, (7), pp. 807–816

[11] Baghayipour, M., Darabi, A., Dastfan, A.: 'Detailed analytical method for predicting the steady-state time variations and entire harmonic contents of principal performance characteristics in a non-slotted axial flux permanent magnet motor, considering a precise iron loss model', *IET Electr. Power Appl.*, 2018, **12**, (3), pp. 308–322

[12] Baghayipour, M., Darabi, A., Dastfan, A.: 'An analytical model of harmonic content no-load magnetic fields and back EMF in axial flux PM machines regarding the iron saturation and winding distribution', *COMPEL – Int. J. Compu. Math. Electr. Electron. Eng.*, 2018, **37**, (1), pp. 54–76

[13] IEC60404-2: 'Magnetic materials – part 2: methods of measurement of the magnetic properties of electrical steel sheet and strip by means of an Epstein frame', 2008

[14] Krings, A.: 'Iron losses in electrical machines – influence of material properties, manufacturing processes, and inverter operation'. PhD Thesis, KTH Royal Inst. Tech., Stockholm, Sweden, 2014

[15] Czichos, H., Saito, T., Smith, L.: '*Handbook of materials measurement methods*' (Springer, Germany, 2006)

[16] IEC62044-3: 'Cores made of soft magnetic materials – measuring methods – part 3: magnetic properties at high excitation level', 2000

[17] Fiorillo, F.: '*Measurement and characterization of magnetic materials*' (Elsevier Academic Press, London, England, 2005)

[18] Lim, M.S., Chai, S.H., Hong, J.P.: 'Design and iron loss analysis of sensorless-controlled interior permanent magnet synchronous motors with concentrated winding', *IET Electr. Power Appl.*, 2014, **8**, (9), pp. 349–356

[19] Nam, H., Ha, K.-H., Lee, J.-J., *et al.*: 'A study on iron loss analysis method considering the harmonics of the flux density waveform using iron loss curves tested on Epstein samples', *IEEE Trans. Magn.*, 2003, **39**, (3), pp. 1472–1475

[20] Lee, B.-H., Kwon, S.-O., Sun, T., *et al.*: 'Modeling of core loss resistance for d-q equivalent circuit analysis of IPMSM considering harmonic linkage flux', *IEEE Trans. Magn.*, 2011, **47**, (5), pp. 1066–1069

[21] Li, J., Abdallah, T., Sullivan, C.: 'Improved calculation of core loss with nonsinusoidal waveforms'. Conf. Rec. 2001 IEEE Ind. Appl. Conf. 36th IAS Ann. Meeting (Cat. No.01CH37248), Chicago, IL, USA, 2001

[22] Venkatachalam, K., Sullivan, C., Abdallah, T., *et al.*: 'Accurate prediction of ferrite core loss with nonsinusoidal waveforms using only Steinmetz parameters'. 2002 IEEE Workshop Comput. Power Electron., Mayaguez, Puerto Rico, USA, 2002

[23] Takeda, Y., Takahashi, Y., Fujiwara, K., *et al.*: 'Iron loss estimation method for rotating machines taking account of hysteretic property', *IEEE Trans. Magn.*, 2015, **51**, (3), pp. 1–4

[24] Lim, M.S., Kim, J.H., Hong, J.P.: 'Experimental characterization of the slinky-laminated core and iron loss analysis of electrical machine', *IEEE Trans. Magn.*, 2015, **51**, (11)

[25] Lim, M.-S., Chai, S.-H., Yang, J.-S., *et al.*: 'Design and verification of 150-krpm PMSM based on experiment results of prototype', *IEEE Trans. Ind. Electron.*, 2015, **62**, (12), pp. 7827–7836